Title

N-linked glycosylation of protease-activated receptor-1 at extracellular loop 2 regulates G-protein signaling bias

Journal

Proceedings of the National Academy of Sciences of the United States of America, 112(27)

ISSN

0027-8424

Authors

Soto, Antonio G
Smith, Thomas H
Chen, Buxin
et al.

Publication Date

2015-07-07

DOI

10.1073/pnas.1508838112

Peer reviewed

N-linked glycosylation of protease-activated receptor-1 at extracellular loop 2 regulates G-protein signaling bias

Antonio G. Soto[a,b,1], Thomas H. Smith[a,b,1], Buxin Chen[a,1], Supriyo Bhattacharya[c], Isabel Canto Cordova[a,b], Terry Kenakin[d], Nagarajan Vaidehi[c], and JoAnn Trejo[a,2]

[a]Department of Pharmacology, School of Medicine, University of California, San Diego, La Jolla, CA 92093; [b]Biomedical Sciences Graduate Program, School of Medicine, University of California, San Diego, La Jolla, CA 92093; [c]Department of Immunology, Beckman Research Institute of the City of Hope, Duarte, CA 91010; and [d]Department of Pharmacology, School of Medicine, University of North Carolina, Chapel Hill, NC 27599

Edited by Robert J. Lefkowitz, Howard Hughes Medical Institute, Duke University Medical Center, Durham, NC, and approved May 19, 2015 (received for review May 6, 2015)

Protease-activated receptor-1 (PAR1) is a G-protein-coupled receptor (GPCR) for the coagulant protease thrombin. Similar to other GPCRs, PAR1 is promiscuous and couples to multiple heterotrimeric G-protein subtypes in the same cell and promotes diverse cellular responses. The molecular mechanism by which activation of a given GPCR with the same ligand permits coupling to multiple G-protein subtypes is unclear. Here, we report that N-linked glycosylation of PAR1 at extracellular loop 2 (ECL2) controls $G_{12/13}$ versus G_q coupling specificity in response to thrombin stimulation. A PAR1 mutant deficient in glycosylation at ECL2 was more effective at stimulating G_q-mediated phosphoinositide signaling compared with glycosylated wildtype receptor. In contrast, wildtype PAR1 displayed a greater efficacy at $G_{12/13}$-dependent RhoA activation compared with mutant receptor lacking glycosylation at ECL2. Endogenous PAR1 rendered deficient in glycosylation using tunicamycin, a glycoprotein synthesis inhibitor, also exhibited increased PI signaling and diminished RhoA activation opposite to native receptor. Remarkably, PAR1 wildtype and glycosylation-deficient mutant were equally effective at coupling to G_i and β-arrestin-1. Consistent with preferential $G_{12/13}$ coupling, thrombin-stimulated PAR1 wildtype strongly induced RhoA-mediated stress fiber formation compared with mutant receptor. In striking contrast, glycosylation-deficient PAR1 was more effective at increasing cellular proliferation, associated with G_q signaling, than wildtype receptor. These studies suggest that N-linked glycosylation at ECL2 contributes to the stabilization of an active PAR1 state that preferentially couples to $G_{12/13}$ versus G_q and defines a previously unidentified function for N-linked glycosylation of GPCRs in regulating G-protein signaling bias.

thrombin | GPCR | arrestin | endothelial | RhoA

Protease-activated receptor-1 (PAR1) is the prototypical member of a family of four G-protein-coupled receptors (GPCRs) that are activated by specific proteases including the coagulant protease thrombin. Thrombin is generated during vascular injury and inflammation and promotes hemostasis, thrombosis, and inflammatory and proliferative responses (1). PAR1 is crucial for thrombin-elicited responses in cell types such as human platelets, fibroblasts, and endothelial cells and accordingly is an important drug target for vascular and thrombotic diseases (2). PAR1 has also been implicated in progression of certain malignant cancers (3).

Thrombin activates PAR1 through proteolytic cleavage of the extracellular N terminus, which unmasks a new N-terminal domain that acts as a tethered ligand that binds intramolecularly to the receptor to induce transmembrane signaling (4, 5). A synthetic peptide that mimics the first six residues of the newly formed N terminus, SFLLRN, can activate PAR1 independent of thrombin and receptor cleavage. Several studies indicate that residues within the tethered ligand sequence interact specifically with residues in the extracellular loop 2 (ECL2) of PAR1 to facilitate receptor activation (6, 7). The high-resolution crystal structure of PAR1 bound to the antagonist vorapaxar also reveals a superficial hydrophobic binding pocket close to the extracellular surface (8). These studies suggest that the PAR1 tethered ligand likely binds superficially to ECL2 to induce conformational changes sufficient for receptor activation.

Once activated by thrombin, PAR1 couples to multiple heterotrimeric G-protein subtypes concomitantly in the same cell. PAR1 stimulates phospholipase C-catalyzed hydrolysis of phosphoinositides (PI) through G_q and inhibits adenylyl cyclase through G_i at the same time (9). Concurrently, PAR1 couples to $G_{12/13}$, leading to activation of Rho guanine nucleotide exchange factors and RhoA signaling (10). Similar to other GPCRs, the intracellular loop 2 (ICL2) and putative eighth helix have been implicated in PAR1 interaction with G proteins (11, 12). In addition, particular residues within ICL2 appear to dictate PAR1–G-protein subtype coupling specificity (13). However, it remains unclear how the tethered ligand of PAR1 generated by thrombin cleavage might interact differently with the receptor to specify unique coupling to distinct G-protein subtypes in the same cell.

GPCRs are dynamic molecules that assume different conformational states. Consequently, different ligands can stabilize unique active conformations of the same GPCR and facilitate activation of distinct signaling effectors such as G proteins or β-arrestins (14, 15). This process is termed biased agonism or functional selectivity. Quantification of GPCR signaling bias has also been shown to describe the effects of receptor mutation on the relative interactions

Significance

G-protein-coupled receptors (GPCRs) are the largest class of mammalian signaling receptors and mediate vast physiological responses. The capacity to modulate GPCR signaling therapeutically is important for treatment of various diseases, and discovering new aspects of receptor signaling is critical for drug development. Protease-activated receptor-1 (PAR1) is GPCR for thrombin. Similar to other GPCRs, PAR1 is promiscuous and couples to multiple heterotrimeric G-protein subtypes in the same cell. How a single GPCR can couple to multiple G-protein subtypes concurrently has remained an enigma. We demonstrate that N-linked glycosylation of PAR1 regulates G-protein coupling specificity and differentially controls cellular responses. Thus, the status of GPCR glycosylation is a critical determinant for specifying coupling to distinct G-protein subtypes.

Author contributions: A.G.S., T.H.S., I.C.C., and J.T. designed research; A.G.S., T.H.S., B.C., and I.C.C. performed research; A.G.S., T.H.S., B.C., S.B., I.C.C., T.K., N.V., and J.T. analyzed data; and A.G.S., S.B., T.K., N.V., and J.T. wrote the paper.

The authors declare no conflict of interest.

This article is a PNAS Direct Submission.

[1]A.G.S., T.H.S., and B.C. contributed equally to this work.

[2]To whom correspondence should be addressed. Email: joanntrejo@ucsd.edu.

This article contains supporting information online at www.pnas.org/lookup/suppl/doi:10.1073/pnas.1508838112/-/DCSupplemental.

with signaling effectors (16, 17). Besides binding of ligands to allosteric sites on the receptor, GPCR interaction with other proteins and segregation into plasma membrane microdomains have been reported to affect receptor bias toward particular effectors. However, whether posttranslational modification of a given GPCR affects ligand-induced coupling to distinct signaling effectors is not known. Here, we report that asparagine (N)-linked glycosylation of PAR1 at ECL2 regulates $G_{12/13}$- versus G_q-protein coupling specificity, which modulates the robustness of thrombin-induced $G_{12/13}$-dependent RhoA mediated stress fiber formation and cellular proliferation associated with G_q signaling in fibroblasts. These findings are the first, to our knowledge, to define a function for N-linked glycosylation of a GPCR in regulating G-protein signaling bias.

Results

PAR1 Deficient in Glycosylation at ECL2 Exhibits Enhanced G_q-Mediated PI Signaling. PAR1 containing amino acid Asn250Ala and Asn259Ala mutations that lacks N-linked glycosylation at ECL2, designated NA ECL2, displayed a greater capacity to stimulate PI hydrolysis compared with wildtype (WT) receptor following exposure to thrombin in HeLa cells (18). Similar differences in thrombin-induced PI hydrolysis were observed in COS-7 cells transiently expressing comparable levels of cell surface PAR1 WT and NA ECL2 mutant (Fig. S1 *A* and *B*). To determine whether activated PAR1 coupling to G_q protein specifically mediates enhanced PI signaling, siRNA was used to deplete cells of $G\alpha_q$ expression (Fig. 1*A*). HeLa cells stably expressing PAR1 WT and NA ECL2 mutant were transfected with nonspecific or $G\alpha_q$-specific siRNAs and labeled with *myo*-[^{3}H]inositol. Thrombin stimulated a greater increase in PI hydrolysis in PAR1 NA ECL2 cells compared with WT cells transfected with nonspecific siRNA that was not due to differences in receptor expression (Fig. 1 *A* and *B*). However, both PAR1 WT and NA ECL2 cells deficient in $G\alpha_q$ expression failed to elicit a thrombin response (Fig. 1*A*), indicating that activated PAR1-induced PI hydrolysis is mediated by G_q in HeLa cells.

To determine if glycosylation of PAR1 at ECL2 affects G_q-stimulated PI signaling by modulating receptor association with $G\alpha_q$ protein, we performed coimmunoprecipitation (co-IP) assays. HeLa cells stably expressing PAR1 WT or NA ECL2 mutant were transiently transfected with different amounts of

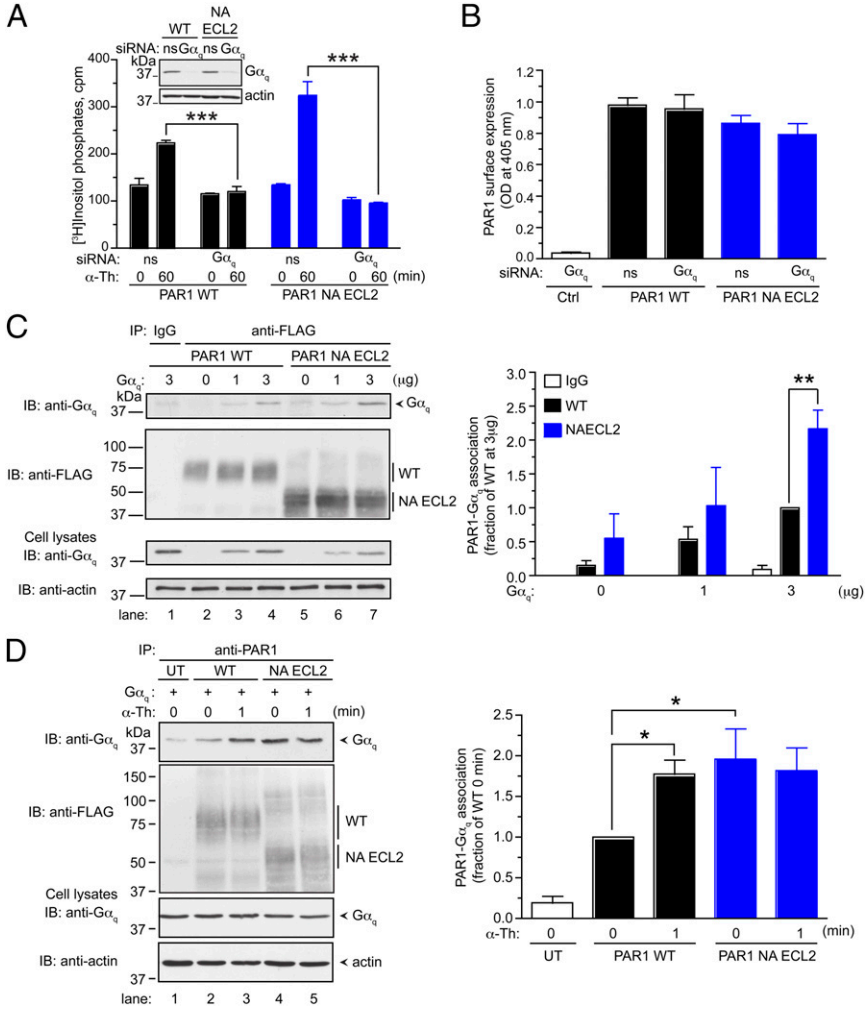

Fig. 1. PAR1 NA ECL2 mutant exhibits enhanced $G\alpha_q$-mediated PI hydrolysis. (*A*) FLAG–PAR1 WT or FLAG–NA ECL2 mutant HeLa cells transfected with nonspecific (ns) or $G\alpha_q$ siRNA labeled with *myo*-[^{3}H]inositol were stimulated with 10 nM α-Th. Data (mean ± SD; $n = 3$) are from three independent experiments and were significant (***$P < 0.001$). (*B*) PAR1 surface expression (mean ± SD; $n = 3$) was determined by ELISA. Control (Ctrl) is secondary antibody only. (*Inset*) Immunoblots of cell lysates. (*C*) FLAG–PAR1 WT or FLAG–NA ECL2 mutant HeLa cells transiently transfected with HA–$G\alpha_q$ were lysed, immunoprecipitated, and immunoblotted as indicated. Data (mean ± SD; $n = 3$) are from three independent experiments and were significant (**$P < 0.01$). (*D*) FLAG–PAR1 WT or FLAG–NA ECL2 mutant HeLa cells transfected with HA–$G\alpha_q$ or untransfected (UT) cells were treated with 10 nM α-Th, lysed, immunoprecipitated, and immunoblotted as indicated. Data (mean ± SEM; $n = 4$) are from four independent experiments and were significant (*$P < 0.01$).

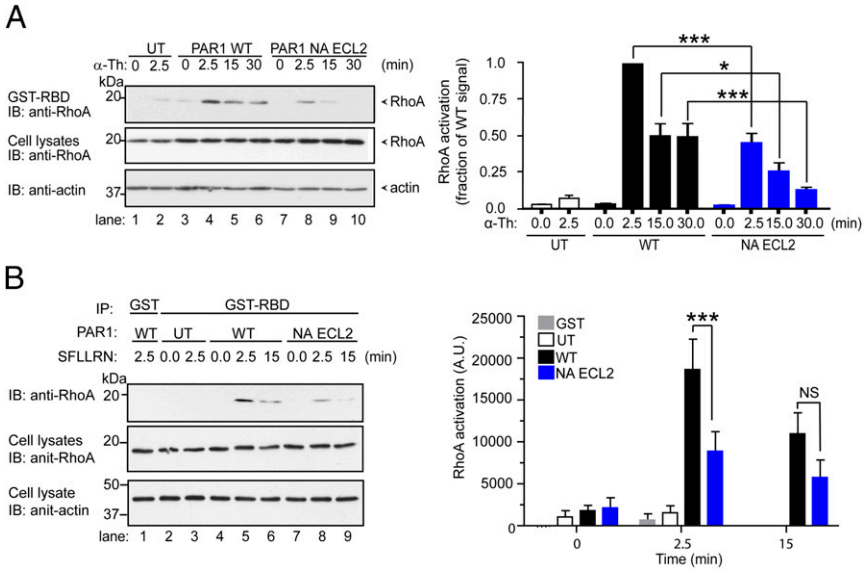

Fig. 2. PAR1 WT and NA ECL2 differentially activate RhoA. FLAG–PAR1 WT and NA ECL2 mutant HeLa cells displaying similar cell surface expression (WT, 0.363 ± 0.079; NA ECL2, 0.363 ± 0.049, OD units) were treated with 10 nM α-Th (*A*) or 100 μM SFLLRN (*B*), lysed, and processed for GST-RBD pull-down assays, and activated RhoA was detected by immunoblotting. UT cells were processed similarly. The data (mean ± SD; $n = 3$) were normalized to total RhoA, are representative of three independent experiments, and were significant (*$P < 0.05$; ***$P < 0.001$). NS, not significant.

$G\alpha_q$ plasmid. PAR1 was immunoprecipitated, and coassociated $G\alpha_q$ was detected by immunoblotting. PAR1 NA ECL2 exhibited a greater capacity to co-IP with $G\alpha_q$ basally compared with WT receptor or IgG control (Fig. 1*C*, lanes 1, 4, and 7). Remarkably, thrombin induced a twofold increase in PAR1 WT–$G\alpha_q$ association compared with control cells (Fig. 1*D*, lanes 1–3). Although PAR1 NA ECL2 mutant exhibited a statistically greater capacity to interact with $G\alpha_q$ basally (Fig. 1 *C* and *D*), receptor–$G\alpha_q$ coassociation was not further increased by thrombin stimulation (Fig. 1*D*, lanes 4 and 5). The PAR1 NA ECL2 mutant expressed in COS-7 cells also showed enhanced association with $G\alpha_q$ protein compared with WT receptor (Fig. S1*C*), indicating that the observed findings are not cell type specific.

In many cell types, PAR1 and G_q localize to caveolae (19, 20), plasma membrane lipid rafts enriched in cholesterol and caveolin-1. To exclude the possibility that altered PAR1 WT versus NA ECL2 mutant activation of G_q protein might be due to differential localization in caveolae, sucrose gradient fractionation was used. A similar distribution of PAR1 WT, NA ECL2, and G_q proteins in caveolin-1 enriched and nonenriched fractions was observed (Fig. S1*D*). These data suggest that thrombin-activated PAR1 lacking glycosylation at ECL2 displays an enhanced capacity to couple to G_q-dependent PI signaling in different cell types that is not due to alterations in receptor expression or distribution to caveolae.

PAR1 NA ECL2 Displays Diminished $G_{12/13}$-Mediated RhoA Signaling. To examine whether glycosylation at ECL2 regulates PAR1 coupling to other G-protein subtypes, we examined RhoA activation, an effector of $G_{12/13}$ proteins. HeLa cells stably expressing comparable PAR1 WT and NA ECL2 at the cell surface were stimulated with thrombin, and activation of RhoA was measured using GST-rhotekin Rho-binding domain (RBD) pull-down assays (21). Thrombin induced a robust increase in RhoA activation at 2.5 min in PAR1 WT cells that subsided after 15–30 min (Fig. 2*A*, lanes 3–6), whereas untransfected cells not expressing PAR1 were not responsive (Fig. 2*A*, lanes 1 and 2). In contrast, RhoA activation was significantly reduced in thrombin-treated PAR1 NA ECL2 cells examined over the same time frame (Fig. 2*A*, lanes 3–10). Consistent with these findings, activated PAR1 WT was more potent at stimulating RhoA activation than the NA ECL2 mutant assessed at earlier time points (Fig. S2*A*). The peptide agonist SFLLRN also significantly increased RhoA activation in PAR1 WT cells compared with NA ECL2 expressing cells (Fig. 2*B*, lanes 4–9), indicating that neither thrombin binding nor proteolytic cleavage contribute to differential RhoA activation. Compared with PAR1 NA ECL2 mutant, RhoA activation induced by thrombin-activated PAR1 WT was also markedly increased in COS-7 cells (Fig. S2*B*). These data suggest that activated PAR1 WT has a greater capacity to induce RhoA signaling compared to mutant receptor deficient in glycosylation at ECL2.

To determine if the differences in RhoA activation exhibited by PAR1 WT versus NA ECL2 mutant are mediated by $G_{12/13}$ proteins, siRNAs were used to deplete cells of $G\alpha_{12}$ and/or $G\alpha_{13}$ expression. PAR1 WT and NA ECL2 mutant-expressing HeLa cells were transfected with nonspecific, $G\alpha_{12}$, $G\alpha_{13}$, or $G\alpha_{12}$ and $G\alpha_{13}$ siRNAs and then stimulated with thrombin. Immunoblotting analysis indicates that siRNAs specifically depleted $G\alpha_{12}$ or $G\alpha_{13}$ protein in PAR1 WT and NA ECL2 cells (Fig. 3 *A* and *B*). Thrombin-activated PAR1 WT caused a significant increase in RhoA activation in nonspecific siRNA control cells that was virtually abolished in cells depleted of either $G\alpha_{12}$ or $G\alpha_{13}$ proteins (Fig. 3*A*, lanes 5–8). The modest increase in RhoA activation observed in thrombin treated PAR1 NA ECL2 siRNA transfected control cells was also significantly inhibited in $G\alpha_{12}$ and $G\alpha_{13}$ knockdown cells (Fig. 3*B*, lanes 5–8). These findings indicate that PAR1-induced RhoA activation is dependent on $G_{12/13}$ proteins.

We next examined if PAR1 WT and NA ECL2 mutant showed differences in $G_{12/13}$ association using co-IP. HeLa cells stably expressing PAR1 WT and NA ECL2 mutant were transiently transfected with increasing amounts of $G\alpha_{12}$ plasmid. Cells were then stimulated with thrombin and immunoprecipitated, and the presence of coassociated $G\alpha_{12}$ protein was detected. PAR1 WT showed greater association with $G\alpha_{12}$ compared with NA ECL2 mutant basally when expressed at low levels (Fig. 4*A*, lanes 1–5 and 7–9) and after thrombin stimulation (Fig. 4*A*, lanes 6 and 10). PAR1 WT also exhibited a preference for $G\alpha_{13}$ association compared with the NA ECL2 mutant both in the presence and absence of thrombin stimulation (Fig. S3). Bioluminescence resonance energy transfer (BRET) measurement

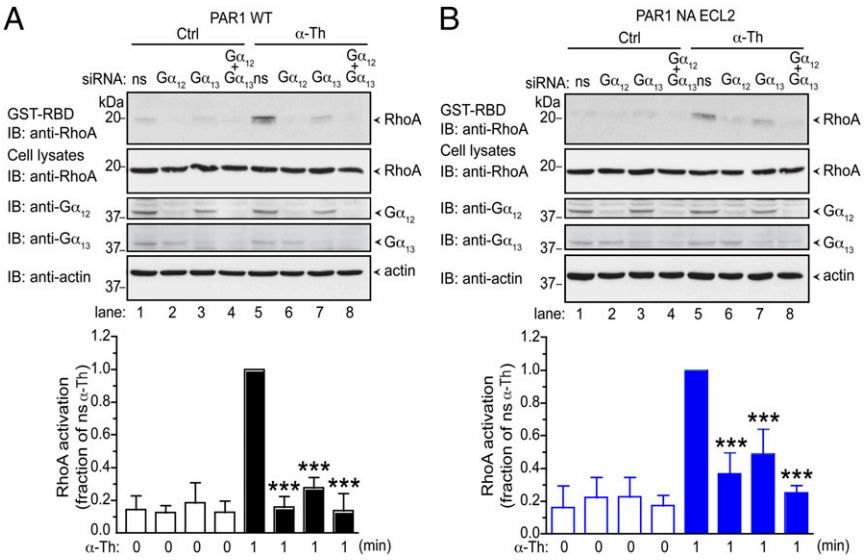

Fig. 3. Thrombin-induced RhoA activation requires $G\alpha_{12}$ and $G\alpha_{13}$ expression. FLAG–PAR1 WT (*A*) or NA ECL2 mutant (*B*) HeLa cells transfected with siRNAs were treated with 10 nM α-Th and processed for GST-RBD pull-down assays, and RhoA activation was determined. Cell lysates were immunoblotted as indicated. Data (mean ± SD; $n = 3$) are from three independent experiments and were significant (***$P < 0.001$).

was also used to assess PAR1–$G\alpha_{12}$ association in living cells. COS-7 cells were transiently transfected with either full-length PAR1 WT or NA ECL2 mutant fused to YFP at the C terminus and $G\alpha_{12}$–Rluc that yielded optimal expression (Fig. S4). Cells were then either left untreated or treated with thrombin, and the net BRET signal was quantified. Thrombin induced a statistically significant increase in the net BRET response elicited by PAR1 WT–YFP and $G\alpha_{12}$–Rluc compared with untreated control cells (Fig. 4*B*), suggesting that the activated PAR1 WT–$G\alpha_{12}$ complex undergoes a conformational change. In contrast, thrombin failed to induce a change in BRET signal in cells coexpressing PAR1 NA ECL2 and $G\alpha_{12}$–Rluc (Fig. 4*B*). These studies suggest that activation of PAR1 glycosylated at ECL2 results in a conformational state that preferentially couples to $G_{12/13}$.

Glycosylation of PAR1 at ECL2 Does Not Affect G_i Coupling or β-arrestin-1 Recruitment. In addition to G_q and $G_{12/13}$, PAR1 is known to signal through the G_i protein in various cell types (1, 9). To investigate whether glycosylation of PAR1 at ECL2 regulates coupling to G_i, we examined PAR1–G_i association by BRET. COS-7 cells were transiently transfected with a constant amount of $G\alpha_i$–Rluc and increasing amounts of either PAR1 WT–YFP or NA ECL2–YFP, and the net BRET was determined. A hyperbolic increase in net BRET was observed as the ratio of PAR1 WT–YFP to $G\alpha_i$–Rluc expression was increased (Fig. 5*A*), suggesting a specific interaction. PAR1 NA ECL2–YFP and $G\alpha_i$–Rluc saturation curves also yielded a hyperbolic increase in the net BRET signal (Fig. 5*A*), suggesting that glycosylation of PAR1 at ECL2 does not affect basal association with G_i protein. We next examined whether thrombin induced a change in PAR1–G_i association. In COS-7 cells coexpressing equivalent amounts of either PAR1 WT–YFP or NA ECL2–YFP together with $G\alpha_i$–Rluc (Fig. S5 *A* and *B*), the addition of thrombin resulted in a rapid and transient increase in net BRET that peaked at 1 min and returned to baseline (Fig. 5*B*). These findings indicate that activated PAR1 coupling to G_i is not affected by glycosylation at ECL2. These results were confirmed by examining PAR1–$G\alpha_i$ association using co-IP. Activation of either PAR1 WT–YFP or NA ECL2–YFP with thrombin resulted in a marked fourfold increase in $G\alpha_i$–Rluc association compared with untreated control cells (Fig. 5*C*), consistent with the equal capacity of both PAR1 WT and NA ECL2 to associate with G_i protein.

In addition to G proteins, many GPCRs display bias toward the multifunctional β-arrestin adaptor proteins (22). Since the β-arrestin-1 isoform is the principal regulator of thrombin-activated PAR1 signaling (23, 24), recruitment of β-arrestin-1 to PAR1 was examined by BRET. Intriguingly, PAR1 WT and NA ECL2 expressed at similar levels were equally effective at recruiting β-arrestin-1 following thrombin stimulation (Fig. 5 *D* and *E* and Fig. S5*C*), indicating that glycosylation does not affect receptor–β-arrestin-1 association. Together, these data suggest that unlike $G_{12/13}$ and G_q, PAR1 deficient in glycosylation at ECL2 displays no bias toward G_i or β-arrestin-1.

Quantifying PAR1 signaling bias. The operational model of agonism was next used to quantify the G-protein coupling bias of PAR1 WT versus NA ECL2 mutant (25, 26). The concentration–response curves of G_q-stimulated PI hydrolysis, $G_{12/13}$-induced RhoA activation, and G_i-activated PAR1 association (BRET) (Fig. S6) were normalized to receptor expression and fitted to the Black–Leff model of agonism to obtain the dissociation constant of the agonist–receptor complex (K_A) and an estimation of the τ transducer constant. The parameters τ and K_A provide an approximation of the signal transduction efficiency and intrinsic agonist efficacy (Tables S1 and S2). The transduction coefficient for each pathway was then calculated as $\log(\tau/K_A)$. To determine the relative bias of PAR1 NA ECL2 mutant to WT receptor, G_i BRET response was used as the reference pathway, because G_i displayed the least difference between WT and NA ECL2 mutant receptor. Each of the PAR1 WT and NA ECL2 mutant G-protein signaling assays were performed in the same cell type with comparable cell surface expression (Fig. S6). To compare thrombin-induced G_q and $G_{12/13}$ signaling pathway bias between the PAR1 WT and NA ECL2 mutant, the $\Delta\Delta\log(\tau/K_A)$ was calculated (Table 1 and Fig. S6). The calculated biases [$\Delta\Delta\log(\tau/K_A)$ values] indicate that PAR1 NA ECL2 mutant is 0.58-fold less effective at coupling to the $G_{12/13}$–RhoA pathway compared with WT receptor, whereas PAR1 NA ECL2 is 5.27-fold more effective at stimulating G_q-induced PI hydrolysis than WT receptor. These findings strongly suggest that N-linked glycosylation of PAR1 at ECL2 regulates $G_{12/13}$-versus G_q-protein bias signaling.

Glycosylation-deficient endogenous PAR1 displays G-protein signaling bias. PAR1 is expressed in endothelial cells and signals through G_q and $G_{12/13}$ to promote inflammatory responses (27). To determine if glycosylation of endogenous PAR1 regulates G-protein signaling bias in human cultured endothelial cells, we used the pharmacological inhibitor tunicamycin, which blocks the first step in glycoprotein synthesis. Glycosylated PAR1 migrates as a broad ~75-kDa protein that was reduced to its predicted molecular weight of ~40 kDa following treatment with tunicamycin (Fig. 6*A*, lanes 3 and 5), consistent with previous studies (18). Tunicamycin also caused partial loss of PAR1 surface expression (Fig. S7*A*); however, the majority of the receptor trafficked to the cell surface. This was confirmed by examining PAR1's susceptibility to cleavage by thrombin at 4 °C (18), which caused a shift in the size of the major PAR1 species in both control and tunicamycin-treated cells (Fig. 6*A*, lanes 3–6). In tunicamycin-treated endothelial cells expressing deglycosylated endogenous PAR1, thrombin induced a significantly greater increase in PI hydrolysis compared with control cells expressing the glycosylated native receptor (Fig. 6*B*). In striking contrast, thrombin caused a marked response in RhoA activation under control conditions that was virtually ablated in cells treated with tunicamycin (Fig. 6*C*). To ensure that tunicamycin does not globally affect cell signaling, epidermal growth factor (EGF)-induced ERK1/2 activation was examined and shown to be equivocal in control and tunicamycin-treated cells (Fig. S7*B*). These findings provide evidence that N-linked glycosylation of PAR1 at ECL2 promotes enhanced G-protein-mediated PI signaling and diminished RhoA activation in a natural context.

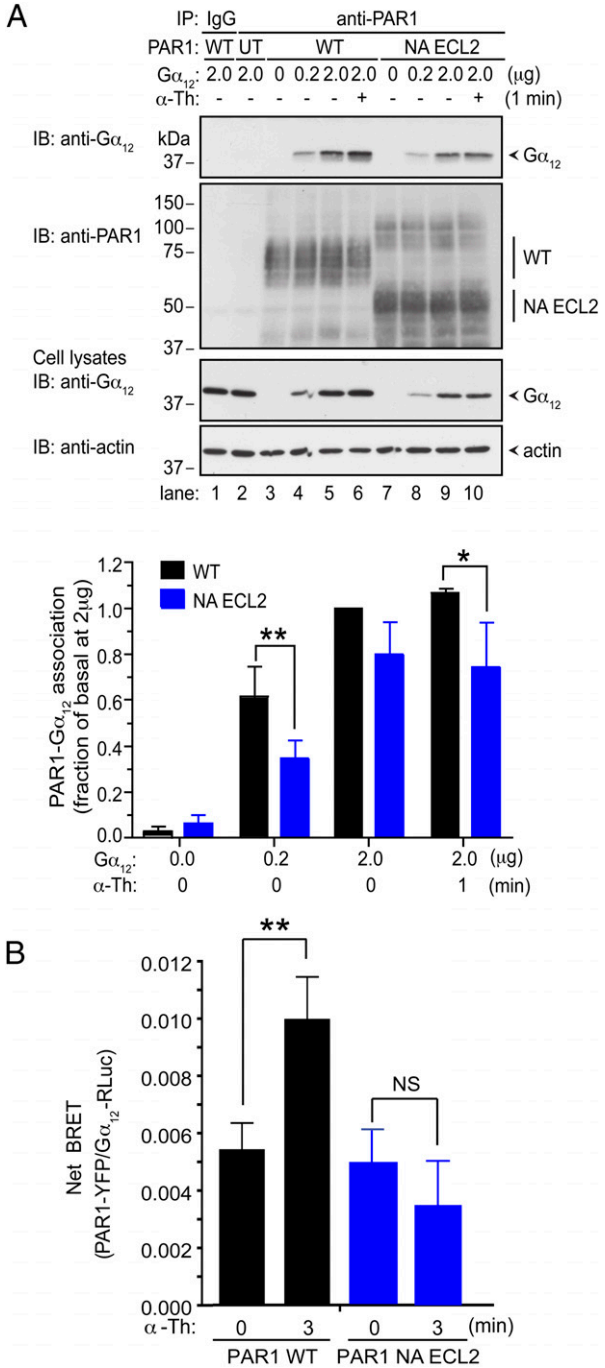

Fig. 4. PAR1 WT and NA ECL2 differentially associate with $G\alpha_{12}$. (*A*) FLAG–PAR1 WT or NA ECL2 HeLa cells transfected with $G\alpha_{12}$–EE were treated with 10 nM α-Th, immunoprecipitated, and immunoblotted. Data (mean ± SD; $n = 3$) are from three independent experiments and were significant (*$P < 0.05$; **$P < 0.01$). (*B*) COS-7 cells cotransfected with PAR1 WT–YFP or NA ECL2–YFP and $G\alpha_{12}$–Rluc were treated with 10 nM α-Th, and BRET was determined. Data shown (mean ± SD; $n = 3$) from three independent experiments were significant (**$P < 0.01$). NS, not significant.

PAR1 NA ECL2 Exhibits Reduced RhoA-Mediated Stress Fiber Formation and Enhanced Cellular Proliferation. To test whether the effects of N-linked glycosylation on PAR1 differential coupling to G_q versus $G_{12/13}$ impacts cellular responses, we examined actin stress fiber formation. Serum-deprived HeLa cells expressing PAR1 WT and NA ECL2 mutant were stimulated with thrombin, stained with phalloidin-TRITC to visualize F-actin filaments and imaged by confocal microscopy. Thrombin caused a marked increase in actin stress fiber formation in PAR1 WT cells (Fig. 7*A*), whereas the response was significantly diminished in NA ECL2 cells (Fig. 7*A*). Inhibition of RhoA activation with C3 toxin virtually abolished thrombin-induced actin stress fiber formation in PAR1 WT cells (Fig. 7*B*), consistent with $G_{12/13}$-induced RhoA-mediated stress fiber formation as previously reported (27). These results suggest that N-linked glycosylation of PAR1 at ECL2 regulates preferential coupling to $G_{12/13}$ and induction of RhoA-mediated stress fiber formation.

Thrombin activation of PAR1 promotes G_q-dependent mitogenic responses in fibroblasts (28, 29). To determine if N-linked glycosylation of PAR1 at ECL2 affects thrombin-induced cellular proliferation, [^{3}H]thymidine incorporation was measured to assess DNA synthesis in fibroblasts. In these studies, mouse lung fibroblasts derived from *Par1*$^{-/-}$ gene knockouts stably expressing PAR1 WT or NA ECL2 mutant were deprived of serum and incubated with thrombin, and the amount of [^{3}H]thymidine incorporation was quantified. Remarkably, fibroblasts expressing PAR1 NA ECL2 displayed a higher basal level of [^{3}H]thymidine incorporation compared with WT fibroblasts (Fig. 7*C*), despite lower cell surface expression of PAR1 NA ECL2 compared with WT receptor (Fig. S7*C*). Moreover, a substantially greater increase in [^{3}H]thymidine incorporation was observed in thrombin-stimulated PAR1 NA ECL2 fibroblasts relative to untreated control or WT fibroblasts (Fig. 7*D*), whereas the cells responded equivocally to serum stimulation (Fig. 7*D*). Together, these findings strongly suggest that N-linked glycosylation of PAR1 at ECL2 regulates preferential coupling to $G_{12/13}$ versus G_q proteins, which modulate the robustness of thrombin-induced cellular responses in various cell types.

Discussion

In the present study, we define a novel function for N-linked glycosylation of a GPCR in regulation of G-protein signaling bias. A PAR1 mutant deficient in glycosylation at ECL2 favored coupling to G_q-mediated PI signaling over $G_{12/13}$-induced

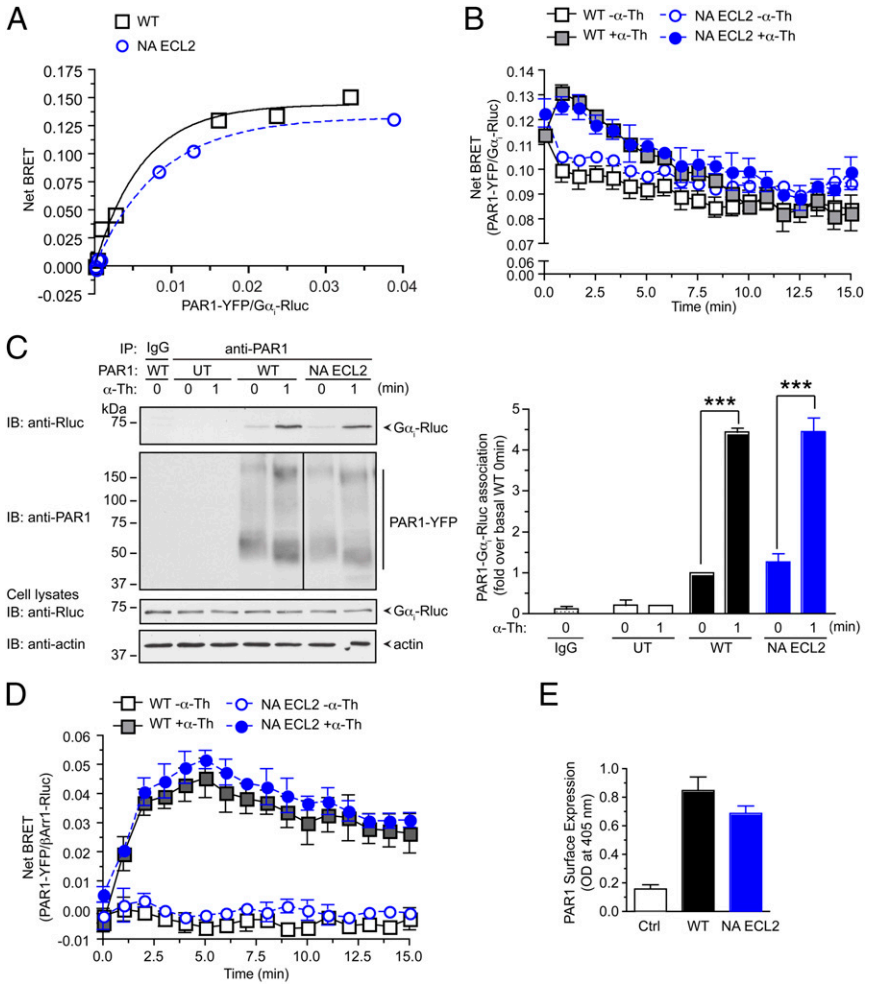

Fig. 5. PAR1 WT and NA ECL2 are equally effective at coupling to G_i and β-arrestin-1. (*A*) COS-7 cells coexpressing increasing PAR1 WT–YFP or NA ECL2–YFP with a constant amount of $G\alpha_i$–Rluc were analyzed by BRET. Data are representative of three independent experiments. (*B*) COS-7 cells coexpressing PAR1 WT–YFP or NA ECL2–YFP and $G\alpha_i$–Rluc were treated with 10 nM α-Th, and BRET was determined. Data (mean ± SD; $n = 3$) are representative of three independent experiments. (*C*) COS-7 cells coexpressing PAR1 WT–YFP or NA ECL2–YFP and $G\alpha_i$–Rluc were stimulated with 10 nM α-Th, immunoprecipitated, and immunoblotted. Data (mean ± SD; $n = 3$) are from three independent experiments and were significant (***$P < 0.001$). (*D*) COS-7 cells coexpressing PAR1 WT–YFP or NA ECL2–YFP and β-arrestin-1–Rluc were stimulated with 10 nM α-Th, and BRET was determined. The data (mean ± SD; $n = 3$) are representative of three independent experiments. (*E*) PAR1 surface expression (mean ± SD; $n = 3$) was measured by ELISA.

RhoA activation, opposite of the glycosylated WT receptor. Moreover, endogenous PAR1 lacking glycosylation exhibited an enhanced G-protein-mediated PI response and reduced RhoA activation, in contrast to native receptor. Intriguingly, both PAR1 WT and mutant were equally effective at coupling to G_i and β-arrestin-1. N-linked glycosylation of PAR1 at ECL2 also enhanced thrombin-induced RhoA-mediated stress fiber formation and attenuated cellular proliferation in fibroblasts, consistent with preferential coupling to $G_{12/13}$ versus G_q proteins. These studies are the first, to our knowledge, to show that N-linked glycosylation of a GPCR is critical for G-protein coupling specificity.

The best described function for N-linked glycosylation of mammalian GPCRs is in proper folding of the nascent protein during translation and export to the cell surface. The majority ~90% of Class A GPCRs contain N-linked glycosylation N–X–S/T consensus sequences within their N terminus, whereas only ~30% of the receptors contain consensus sites within the extracellular loops (30). The extent of glycosylation and full utilization of consensus sites likely varies with a given GPCR. PAR1 contains five consensus sites for N-linked glycosylation, three in the N terminus and two in ECL2, and all appear to be modified by glycosylation (18). We previously showed that glycosylation of PAR1 at the N terminus and not the ECL2 is important for efficient transport to the cell surface (18). In addition to cell surface export, other studies suggest a function for N-linked glycosylation in GPCR dimerization. N-linked glycosylation was shown to contribute to the stabilization of bradykinin-B2 receptor homodimerization (31), whereas β_1-and α_2-adrenergic receptor (AR) heterodimerization was inhibited by glycosylation (32). Although PAR1 NA ECL2 appears largely as a monomer based on immunoblotting analysis (Figs. 1, 4, and 5), a minor higher molecular weight species was sometimes evident. However, we failed to confirm a difference in PAR1 WT versus NA ECL2 mutant dimerization. Another study reported that N-linked glycosylation of the sphingosine-1-phosphate receptor effects caveolae localization (33). Surprisingly, PAR1 distribution into caveolae was not affected by loss of glycosylation at ECL2 (Fig. S1*D*). Thus, these findings suggest that glycosylation of PAR1 at ECL2 likely serves a distinct function not related to surface export, dimerization, or partitioning into caveolae.

Glycosylation can also influence GPCR–ligand interactions. PAR2, a GPCR related to PAR1, is cleaved and activated by trypsin-like serine proteases but not by thrombin (1). N-linked

Table 1. PAR1 WT and NA ECL2 mutant bias coefficients

	PAR1 WT		PAR1 NA ECL2			
Pathway	$\log(\tau/K_A)$	$\Delta\log(\tau/K_A)$	$\log(\tau/K_A)$	$\Delta\log(\tau/K_A)$	$\Delta\Delta\log(\tau/K_A)$	Bias, ±95% c.i.
G_i (ref.)	8.35 ± 0.23		8.14 ± 0.23			
RhoA	9.54 ± 0.23	1.19 ± 0.3	9.09 ± 0.23	0.95 ± 0.3	−0.24 ± 0.42	0.58, 0.22–1.54
PI hydrolysis	8.53 ± 0.20	0.18 ± 0.3	9.04 ± 0.20	0.90 ± 0.3	0.72 ± 0.42	5.27, 1.98–13.98

The operational model of agonism was used to quantify PAR1 WT versus NA ECL2 mutant bias toward $G_{12/13}$-induced RhoA activation and G_q-stimulated PI hydrolysis. The G_i pathway exhibits the least bias and was designated as the reference pathway (ref.). The $\Delta\Delta\log(\tau/K_A)$ value is a measure of the calculated bias for each pathway, with errors corresponding to 95% confidence interval (c.i.).

glycosylation of PAR2 at the N terminus was shown to affect tryptase but not trypsin cleavage (34), indicating that glycosylation directly affects protease recognition and receptor activation. We previously showed that N-linked glycosylation of PAR1 at either the N terminus or ECL2 has no effect on the rate of receptor cleavage by thrombin (18). Intriguingly, differential glycosylation of the gonadotrophin follicle-stimulating hormone (FSH) ligand modulates the capacity of the cognate FSH receptor to couple to G_s versus G_i signaling (35). These findings indicate that naturally occurring heterogeneity of glycosylation of certain peptide hormones can affect GPCR-biased signaling. However, whether naturally occurring glycosylation of GPCRs affects G-protein signaling bias has not been previously reported.

Significant efforts have been made toward understanding the mechanisms by which certain GPCRs couple to multiple distinct G-protein subtypes in the same cell, but it remains poorly understood. Our results suggest that N-linked glycosylation of PAR1 at ECL2 regulates G-protein coupling specificity. The ECL2 of other class A GPCRs has also been shown to control ligand-directed effects (36, 37). Thus, we hypothesize that N-linked glycosylation of PAR1 at ECL2 provides structural diversity that influences ligand–receptor interaction that favors coupling to $G_{12/13}$ versus G_q proteins. The observed PAR1 WT and NA ECL2 mutant bias signaling is not due to alterations in expression of PAR1, G proteins, or intracellular effectors, because differential signaling was seen in the same cell types. In addition, the $\Delta\Delta\text{Log}(\tau/K_A)$ index is a normalized number that takes into account differences in expression (26). Specifically, the effects were expressed in terms of a reference pathway, namely, activation of G_i protein where the mutation caused minimal effect (26). Thus, our studies support a role for N-linked glycosylation in stabilization of a distinct active PAR1 state that selectively couples to $G_{12/13}$ over G_q protein, but has no influence on receptor coupling to G_i or β-arrestin-1. Prior studies showed a role for phosphorylation in isoproterenol-stimulated β_2–AR switching from G_s to G_i (38). In this case, β_2–AR initial coupling to G_s is required for protein kinase A-mediated phosphorylation of ICL3 that promotes coupling to G_i. In contrast to the β_2–AR, we show that the existing status of PAR1 N-linked glycosylation before ligand stimulation is critical for specifying coupling to distinct G-protein subtypes.

Our studies suggest that PAR1 is likely to exist as an ensemble of active states that use different molecular determinants to couple to distinct G-protein subtypes that are stabilized in part by N-linked glycosylation at ECL2. Surprisingly, a role for glycosylation in modulating GPCR allostery and signaling has not been previously explored. The heterogeneity of glycosylation indicates that GPCRs are likely to exist as populations of receptors containing distinct glycan structures even when expressed in the same cell (39). The contribution of these diverse structures to GPCR

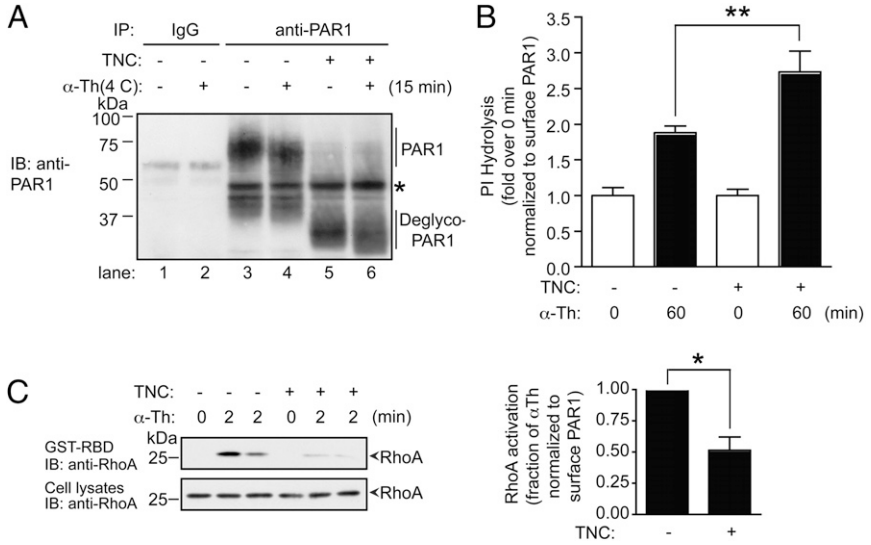

Fig. 6. Glycosylation-deficient endogenous PAR1 exhibits enhanced PI hydrolysis and diminished RhoA activation. (*A*) Endothelial cells incubated with 0.25 μg/mL tunicamycin (TNC) for 18 h and treated with 10 nM α-Th. Cells were lysed, immunoprecipitated, and immunoblotted. Asterisk (*) is a nonspecific band. (*B*) TNC-treated and untreated endothelial cells labeled with *myo*-[^{3}H]inositol were stimulated with 10 nM α-Th, and [^{3}H]IPs were measured. Data (mean ± SD; $n = 3$) were normalized to PAR1 surface expression from three independent experiments and were significant (**$P < 0.01$). (*C*) Endothelial cells treated with or without TNC and 10 nM α-Th were processed for GST-RBD pull-down assays, and RhoA activation was determined. Data (mean ± SD, $n = 4$) were normalized to PAR1 surface expression and were significant (*$P < 0.05$).

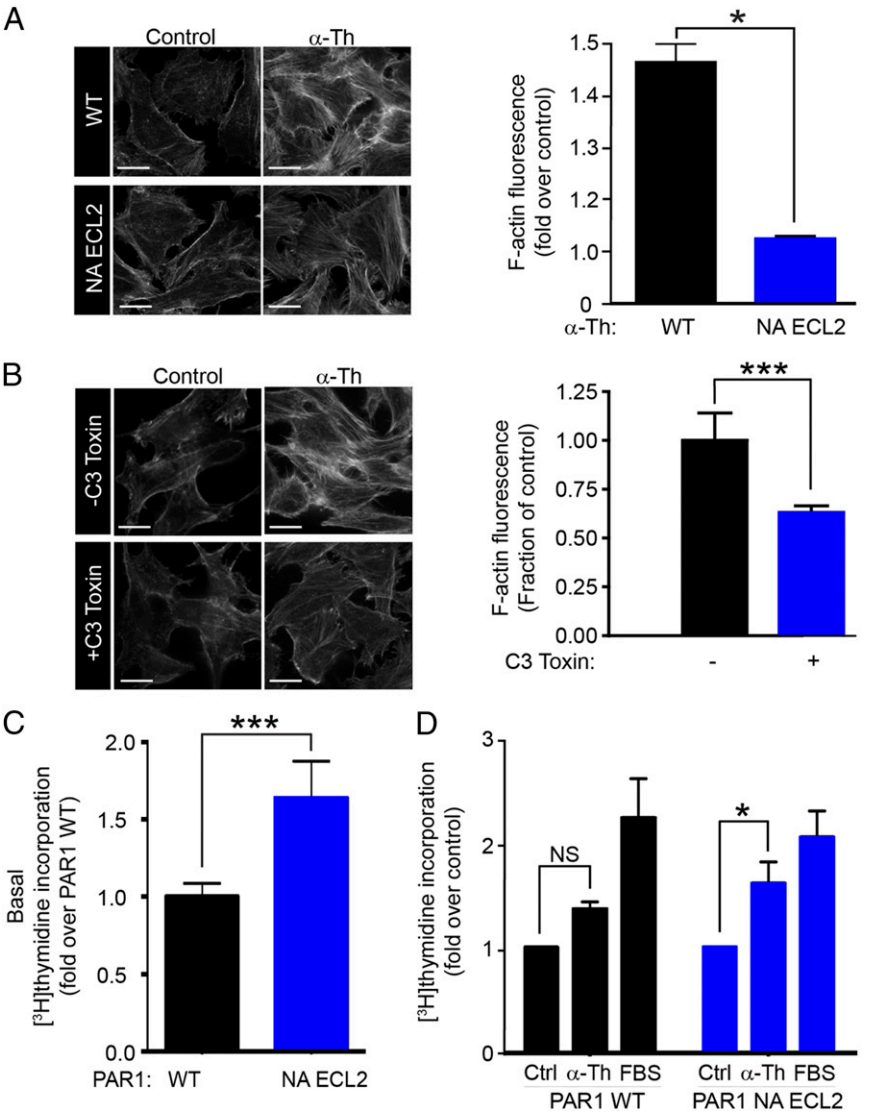

Fig. 7. PAR1 NA ECL2 exhibits diminished stress fiber formation and enhanced cellular proliferation. (*A*) FLAG–PAR1 WT or FLAG–NA ECL2 mutant HeLa cells were treated with 10 nM α-Th for 5 min, stained with phalloidin-TRITC, and imaged. Data (mean ± SD; $n = 3$) for f-actin fluorescence were quantified from four different images of three independent experiments and were significant (*$P < 0.05$). (Scale bar, 10 μm.) (*B*) FLAG–PAR1 WT HeLa cells pretreated with 1.5 μg/mL C3 toxin for 4 h at 37 °C or DMSO were incubated with 10 nM α-Th for 5 min and stained with phalloidin-TRITC, and f-actin fluorescence was quantified. Data (mean ± SD; $n = 3$) were significant (***$P < 0.001$). (Scale bar, 10 μm.) (*C*) Mouse lung fibroblasts expressing FLAG–PAR1 WT or NA ECL2 mutant were incubated without (basal) or (*D*) with 10 nM α-Th or 2% FBS, and [^{3}H]thymidine incorporation was measured. Basal [^{3}H]thymidine incorporation (mean ± SD; $n = 3$) is from three independent experiments and was significant (***$P < 0.001$). Data (mean ± SD; $n = 3$) are from α-Th-stimulated [^{3}H]thymidine incorporation from three independent experiments and were significant (*$P < 0.05$). NS, not significant.

function is not known. PAR1 is extensively glycosylated but the nature and diversity of N-glycan modification have not been determined. Importantly, naturally occurring mutations in N-linked glycosylation consensus sequences of Rhodopsin have been linked to retinitis pigmentosa (40, 41), indicating that modulation of GPCR glycosylation status can contribute to disease progression. However, mutations in PAR1 N-linked glycosylation sites have not been identified. In summary, our findings demonstrate for the first time, to our knowledge, that N-linked glycosylation of a GPCR specifies coupling to distinct G-protein subtypes in the same cell.

Materials and Methods

Reagents and Antibodies. Human α-thrombin (α-Th) was from Enzyme Research Laboratories. SFLLRN was synthesized at Tufts University Core Facility. Insulin, transferrin, selenous acid (ITS) premix, caveolin-1, and anti-early endosomal antigen-1 (EEA1) antibodies were from BD Biosciences. ERK1/2 antibodies were from Cell Signaling Technologies. C3 transferase toxin was from Cytoskeleton, Inc. Polyclonal and M2 monoclonal anti-FLAG antibody, TRITC-conjugated phalloidin, tunicamycin, EGF, and anti-β-actin antibody were from Sigma. The anti-PAR1 WEDE antibody was from Beckman Coulter. Anti-PAR1 polyclonal antibody was generated against the YEPFWEDEEKNESGLTEYC peptide. RhoA, $G\alpha_{q/11}$, $G\alpha_{12}$, and $G\alpha_{13}$ antibodies were from Santa Cruz Biotechnology. Renilla Luciferase antibody was from Millipore. Horseradish peroxidase (HRP)-conjugated goat anti-mouse and anti-rabbit antibodies were from Bio-Rad Laboratories.

cDNAs and Cell Lines. HeLa cells stably expressing N-terminal FLAG-tagged PAR1 WT and NA ECL2 were generated as described in ref. 18. HA–$G\alpha_q$ plasmid was from Philip Wedegaertner, Thomas Jefferson University, Philadelphia, PA. $G\alpha_{12}$–EE and $G\alpha_{13}$–EE constructs were from Dr. John Hepler, Emory University, Atlanta, GA. $G\alpha_i$–Rluc, $G\alpha_{12}$–Rluc, $G\alpha_{13}$–Rluc, and PAR1–YFP plasmids were from Dr. Jean-Philippe Pin, Montpellier University, Montpellier, France. PAR1–YFP NA ECL2 mutant was generated by site-directed mutagenesis using the QuikChange Mutagenesis kit (Stratagene) and confirmed by dideoxy sequencing. COS-7, HeLa, and endothelial cells were cultured as described in refs. 18, 21, and 42.

Cell Transfections. See *SI Materials and Methods*.

PAR1 Immunoprecipitation and Immunoblotting. Equivalent amounts of lysates from cells grown in six-well plates were processed for PAR1 immunoprecipitation as described in ref. 18.

PAR1 Cell Surface ELISA. HeLa and COS-7 cells expressing FLAG–PAR1 WT or NA ECL2 mutant were grown in 24-well plates and processed for cell surface ELISA as described in ref. 18.

PI Hydrolysis. Cells were labeled overnight with 1 μCi/mL of *myo*-[^{3}H]inositol (American Radiolabeled Chemicals) and treated with agonists, and accumulated [^{3}H]IPs were measured as described in ref. 18.

BRET Assays. COS-7 cells transiently expressing PAR1 WT–YFP or NA ECL2–YFP and either G protein–Rluc or β-arrestin-1–Rluc were treated with agonists and analyzed by BRET as described in ref. 42.

RhoA Activity Assay. Equivalent amounts of lysates were used for GST-RBD pull-down assays as described in ref. 19.

Calculation of Bias Coefficients. See *SI Materials and Methods*.

Phalloidin Staining. See *SI Materials and Methods*.

[^{3}H]Thymidine Incorporation. See *SI Materials and Methods*.

Data Analysis. Data were analyzed by GraphPad Prism 4.0 software. Statistical analysis was determined by performing Student's *t* test, one-way ANOVA and Dunnett's multiple test, or two-way ANOVA and Bonferroni posttest. Data fitting to the operational model of agonism was performed using MATLAB.

ACKNOWLEDGMENTS. We thank members of the J.T. laboratory for comments and advice. This work was supported by National Institutes of Health (NIH) R01 GM090689 (to J.T.) and AHA Grant-In-Aid 18630018 (to J.T.). A.G.S. was supported by an NIH/National Institute of Heart, Lung, and Blood Institute (NHLBI) Diversity Supplement; I.C.C. was supported by a University of California TRDRP Predoctoral Fellowship; T.H.S. is supported by an NIH/NHLBI F31 Predoctoral Fellowship; and N.V. is supported by NIH R01 GM097261.

1. Coughlin SR (2005) Protease-activated receptors in hemostasis, thrombosis and vascular biology. *J Thromb Haemost* 3(8):1800–1814.
2. Ramachandran R, Noorbakhsh F, Defea K, Hollenberg MD (2012) Targeting proteinase-activated receptors: Therapeutic potential and challenges. *Nat Rev Drug Discov* 11(1):69–86.
3. Arora P, Ricks TK, Trejo J (2007) Protease-activated receptor signalling, endocytic sorting and dysregulation in cancer. *J Cell Sci* 120(Pt 6):921–928.
4. Vu TK, Hung DT, Wheaton VI, Coughlin SR (1991) Molecular cloning of a functional thrombin receptor reveals a novel proteolytic mechanism of receptor activation. *Cell* 64(6):1057–1068.
5. Vu TK, Wheaton VI, Hung DT, Charo I, Coughlin SR (1991) Domains specifying thrombin-receptor interaction. *Nature* 353(6345):674–677.
6. Gerszten RE, et al. (1994) Specificity of the thrombin receptor for agonist peptide is defined by its extracellular surface. *Nature* 368(6472):648–651.
7. Nanevicz T, et al. (1995) Mechanisms of thrombin receptor agonist specificity. Chimeric receptors and complementary mutations identify an agonist recognition site. *J Biol Chem* 270(37):21619–21625.
8. Zhang C, et al. (2012) High-resolution crystal structure of human protease-activated receptor 1. *Nature* 492(7429):387–392.
9. Hung DT, Wong YH, Vu T-KH, Coughlin SR (1992) The cloned platelet thrombin receptor couples to at least two distinct effectors to stimulate phosphoinositide hydrolysis and inhibit adenylyl cyclase. *J Biol Chem* 267(29):20831–20834.
10. McLaughlin JN, et al. (2005) Functional selectivity of G protein signaling by agonist peptides and thrombin for the protease-activated receptor-1. *J Biol Chem* 280(26): 25048–25059.
11. Verrall S, et al. (1997) The thrombin receptor second cytoplasmic loop confers coupling to Gq-like G proteins in chimeric receptors. Additional evidence for a common transmembrane signaling and G protein coupling mechanism in G protein-coupled receptors. *J Biol Chem* 272(11):6898–6902.
12. Swift S, et al. (2006) Role of the PAR1 receptor 8th helix in signaling: The 7-8-1 receptor activation mechanism. *J Biol Chem* 281(7):4109–4116.
13. McCoy KL, et al. (2012) Protease-activated receptor 1 (PAR1) coupling to $G_{q/11}$ but not to $G_{i/o}$ or $G_{12/13}$ is mediated by discrete amino acids within the receptor second intracellular loop. *Cell Signal* 24(6):1351–1360.
14. Kenakin T, Christopoulos A (2013) Signalling bias in new drug discovery: Detection, quantification and therapeutic impact. *Nat Rev Drug Discov* 12(3):205–216.
15. Urban JD, et al. (2007) Functional selectivity and classical concepts of quantitative pharmacology. *J Pharmacol Exp Ther* 320(1):1–13.
16. Tschammer N, Bollinger S, Kenakin T, Gmeiner P (2011) Histidine 6.55 is a major determinant of ligand-biased signaling in dopamine D2L receptor. *Mol Pharmacol* 79(3):575–585.
17. Belmer A, et al. (2014) Role of the N-terminal region in G protein-coupled receptor functions: Negative modulation revealed by 5-HT2B receptor polymorphisms. *Mol Pharmacol* 85(1):127–138.
18. Soto AG, Trejo J (2010) N-linked glycosylation of protease-activated receptor-1 second extracellular loop: A critical determinant for ligand-induced receptor activation and internalization. *J Biol Chem* 285(24):18781–18793.
19. Soh UJ, Trejo J (2011) Activated protein C promotes protease-activated receptor-1 cytoprotective signaling through β-arrestin and dishevelled-2 scaffolds. *Proc Natl Acad Sci USA* 108(50):E1372–E1380.
20. Oh P, Schnitzer JE (2001) Segregation of heterotrimeric G proteins in cell surface microdomains. G_q binds caveolin to concentrate in caveolae, whereas G_i and G_s target lipid rafts by default. *Mol Biol Cell* 12(3):685–698.
21. Russo A, Soh UJ, Paing MM, Arora P, Trejo J (2009) Caveolae are required for protease-selective signaling by protease-activated receptor-1. *Proc Natl Acad Sci USA* 106(15):6393–6397.
22. Reiter E, Ahn S, Shukla AK, Lefkowitz RJ (2012) Molecular mechanism of β-arrestin-biased agonism at seven-transmembrane receptors. *Annu Rev Pharmacol Toxicol* 52:179–197.
23. Goel R, Phillips-Mason PJ, Raben DM, Baldassare JJ (2002) α-thrombin induces rapid and sustained Akt phosphorylation by β-arrestin1-dependent and -independent mechanisms, and only the sustained Akt phosphorylation is essential for G1 phase progression. *J Biol Chem* 277(21):18640–18648.
24. Paing MM, Stutts AB, Kohout TA, Lefkowitz RJ, Trejo J (2002) β-arrestins regulate protease-activated receptor-1 desensitization but not internalization or down-regulation. *J Biol Chem* 277(2):1292–1300.
25. Black JW, Leff P (1983) Operational models of pharmacological agonism. *Proc R Soc Lond Ser B* 220(1219):141e162.
26. Kenakin T, Watson C, Muniz-Medina V, Christopoulos A, Novick S (2012) A simple method for quantifying functional selectivity and agonist bias. *ACS Chem Neurosci* 3(3):193–203.
27. Gilchrist A, et al. (2001) G alpha minigenes expressing C-terminal peptides serve as specific inhibitors of thrombin-mediated endothelial activation. *J Biol Chem* 276(28): 25672–25679.
28. LaMorte VJ, Harootunian AT, Spiegel AM, Tsien RY, Feramisco JR (1993) Mediation of growth factor induced DNA synthesis and calcium mobilization by G_q and G_{i2}. *J Cell Biol* 121(1):91–99.
29. Trejo J, Connolly AJ, Coughlin SR (1996) The cloned thrombin receptor is necessary and sufficient for activation of mitogen-activated protein kinase and mitogenesis in mouse lung fibroblasts. Loss of responses in fibroblasts from receptor knockout mice. *J Biol Chem* 271(35):21536–21541.
30. Landolt-Marticorena C, Reithmeier RA (1994) Asparagine-linked oligosaccharides are localized to single extracytosolic segments in multi-span membrane glycoproteins. *Biochem J* 302(Pt 1):253–260.
31. Xu J, et al. (2003) Heterodimerization of α_{2A}- and β_1-adrenergic receptors. *J Biol Chem* 278(12):10770–10777.
32. Michineau S, Alhenc-Gelas F, Rajerison RM (2006) Human bradykinin B2 receptor sialylation and N-glycosylation participate with disulfide bonding in surface receptor dimerization. *Biochemistry* 45(8):2699–2707.
33. Kohno T, Igarashi Y (2004) Roles for N-glycosylation in the dynamics of Edg-1/S1P1 in sphingosine 1-phosphate-stimulated cells. *Glycoconj J* 21(8-9):497–501.
34. Compton SJ, Sandhu S, Wijesuriya SJ, Hollenberg MD (2002) Glycosylation of human proteinase-activated receptor-2 (hPAR2): Role in cell surface expression and signalling. *Biochem J* 368(Pt 2):495–505.
35. Arey BJ, et al. (1997) Induction of promiscuous G protein coupling of the follicle-stimulating hormone (FSH) receptor: A novel mechanism for transducing pleiotropic actions of FSH isoforms. *Mol Endocrinol* 11(5):517–526.
36. Bokoch MP, et al. (2010) Ligand-specific regulation of the extracellular surface of a G-protein-coupled receptor. *Nature* 463(7277):108–112.
37. Ahuja S, et al. (2009) Helix movement is coupled to displacement of the second extracellular loop in rhodopsin activation. *Nat Struct Mol Biol* 16(2):168–175.
38. Daaka Y, Luttrell LM, Lefkowitz RJ (1997) Switching of the coupling of the β_2-adrenergic receptor to different G proteins by protein kinase A. *Nature* 390(6655):88–91.
39. Ohtsubo K, Marth JD (2006) Glycosylation in cellular mechanisms of health and disease. *Cell* 126(5):855–867.
40. van den Born LI, et al. (1994) Thr4Lys rhodopsin mutation is associated with autosomal dominant retinitis pigmentosa of the cone-rod type in a small Dutch family. *Ophthalmic Genet* 15(2):51–60.
41. Sullivan LJ, et al. (1993) A new codon 15 rhodopsin gene mutation in autosomal dominant retinitis pigmentosa is associated with sectorial disease. *Arch Ophthalmol* 111(11):1512–1517.
42. Lin H, Trejo J (2013) Transactivation of the PAR1-PAR2 heterodimer by thrombin elicits β-arrestin-mediated endosomal signaling. *J Biol Chem* 288(16):11203–11215.

Supporting Information

Soto et al. 10.1073/pnas.1508838112

SI Materials and Methods

Cell Transfections. HeLa cells were transiently transfected with cDNA plasmids using Polyethylenimine (Polysciences Inc.). COS-7 cells were transfected with plasmids using FuGENE 6. PAR1 WT or NA ECL2 mutant HeLa cells were transfected with 100 nM nonspecific or $G_{q/11}$-specific siRNAs or with 50 nM nonspecific siRNA or $G\alpha_{12}$ and $G\alpha_{13}$ siRNAs using Oligofectamine according to the manufacturer's instructions. The nonspecific siRNA 5′-CUACGUCCAGGAGCGCACC-3′ and $G_{q/11}$-specific siRNA 5′-GAUGUUCGUGGACCUGAAC-3′ were from Dharmacon. The $G\alpha_{12}$ siRNA 5′-GGAUCGGCCAGCUGAAUUATT-3′ and $G\alpha_{13}$ siRNA 5′-CGACUGCUUACCAAAUUAATT-3′ were from Qiagen.

Phalloidin Staining. FLAG–PAR1 WT or NA ECL2 mutant HeLa cells were plated on fibronectin-coated glass coverslips in 12-well dishes, serum starved, and then treated with agonist. Cells were washed, fixed with 4% (wt/vol) paraformaldehyde (PFA), permeabilized with 0.5% (vol/vol) Triton X-100 and incubated with 7% (vol/vol) FBS diluted in PBS for 30 min. Cells were washed, stained with Phalloidin-TRITC diluted 1:1,000 in 7% (vol/vol) FBS in PBS for 1 h, and processed for confocal microscopy as described in ref. 18. Images were collected using an Olympus disk spinning unit confocal microscope configured with a PlanApo 60× oil objective and a Hamamatsu ORCA-ER camera. Fluorescent images of X–Y sections at 0.28 μm were collected and mean fluorescence was determined using Intelligent Imaging Innovations Slidebook 4.2 software.

Mouse lung *Par1*$^{-/-}$ fibroblasts stably expressing FLAG–PAR1 WT or FLAG–NA ECL2 mutant were grown in 12-well plates. Cells were incubated with agonists in phenol red-free DMEM containing BSA. After 24 h, fresh phenol red-free DMEM containing agonists and 0.5 μCi/well of [^{3}H]thymidine, 3 μM thymidine, insulin, transferrin, sodium selenite, and BSA was added. After 24 h, cells were washed, precipitated with trichloroacetic acid as described in ref. 29, and solubilized with 0.1 N NaOH, and the amount of [^{3}H]thymidine incorporation was determined by liquid scintillation counting.

Calculation of PAR1 Bias Coefficients. Using the concentration–response curves for thrombin-stimulated PI hydrolysis, RhoA activation, and Gi BRET assay, we calculated the response per cell by dividing the measured response values by the receptor expression. The concentration–response curves were then fitted to the Black–Leff model of agonism (25),

$$\text{Response} - \text{Basal} = \frac{[A]^n \tau^n (E_m - \text{Basal})}{[A]^n \tau^n + ([A] + K_A)^n}, \qquad \text{[S1]}$$

where $[A]$ is the agonist concentration, τ is equal to R_T/K_E (R_T, receptor density; K_E, intrinsic agonist efficacy), n is the transducer slope, and E_m is the maximal response of the system. The transduction coefficient for each pathway was calculated as $\log(\tau/K_A)$ (14). For fitting the data, the Black–Leff equation was recast to a different form according to ref. 16, and $\log(\tau/K_A)$ was directly obtained from the fit. E_m was estimated as the maximum value of the signaling response including both the WT and NA ECL2 mutant PAR1. Setting the value of $n = 1$ gives a good fit for all of the dose–response data. In practice, n was allowed to vary within a very narrow range (0.9–1.2) to account for statistical variability. The fitting was performed using the Genetic Algorithm module in MATLAB (operational model fitting of GraphPad Prism did not always find a solution for all datasets). Instead of starting from a single initial guess of the solution, 10,000 initial guesses were randomly generated within a prescribed range. The provided range for K_A was 10^{-15} to 1, whereas, for $\log(\tau/K_A)$, it was 0–15 (range for n is stated earlier). Using the different initial guesses, the algorithm converged to a solution within the provided tolerance limit of 10^{-8}. The fitted parameters are given in Table S1.

To estimate how the bias changes upon receptor mutation for two assays measuring the response to two signaling pathways, the standard method is to compare signaling response of the WT and mutant receptor for two different agonists, one of the agonists being the reference agonist (16, 17). This cancels out the effects of varying receptor expression and cell-specific differences arising from using different cell assays. In our case, because only one agonist thrombin is available, comparing with a reference agonist was not possible. However, the expression levels of both PAR1 WT and NA ECL2 mutant were similar within statistical error (see Fig. S6). This, combined with the fact that each of the signaling assays comparing WT and NA ECL2 mutant responses were performed in the same cell lines, indicates that the receptor expression and cell-specific differences are minimal. Therefore, the calculated $\log(\tau/K_A)$ values are comparable between the WT and NA ECL2 mutant PAR1. A further normalization was achieved by comparing the signaling effects of the pathways to a common pathway. To calculate the relative bias of the PAR1 WT to NA ECL2 mutant, we designated the G_i pathway as the reference pathway, and calculated the bias of the other signaling pathways relative to the G_i pathway. We selected the G_i pathway as the reference because it shows the minimal bias between the WT and mutant PAR1. For a given pathway, $\Delta\log(\tau/K_A)$ was calculated as $\log(\tau/K_A) - \log(\tau/K_A)_{\text{ref}}$, where $\log(\tau/K_A)_{\text{ref}}$ is the value for the reference G_i pathway. $\Delta\Delta\log(\tau/K_A)$ was then calculated as $\Delta\log(\tau/K_A)_{\text{MUT}} - \Delta\log(\tau/K_A)_{\text{WT}}$. Thus, bias is given by $10^{\Delta\Delta\log(\tau/KA)}$. The calculated $\log(\tau/K_A)$ and the corresponding bias values and error estimates are given in Table 1 and Table S2. Thus, for equal potency of the PAR1 WT and NA ECL2 mutant for the G_i pathway, PAR1 NA ECL2 shows 0.58-fold less activation of the $G_{12/13}$ (RhoA) pathway and 5.27-fold increase in the activation of the G_q (PI hydrolysis) pathway.

To estimate the variability in the calculated $\log(\tau/K_A)$ values, we calculated S_{ij}^2 for receptor i and pathway j as

$$S_{ij}^2 = \frac{1}{n_{ij} - 1} \sum_{k=1}^{n_j} \left(y_{ijk} - y_{mean}\right)^2, \qquad \text{[S2]}$$

where k denotes the number of experiments and y corresponds to the $\log(\tau/K_A)$ for the receptor/pathway pair. The total variability of the estimates S_{pooled} is given by

$$S_{pooled} = \sqrt{\frac{\sum_{i=1}^{2}\sum_{j=1}^{3} S_{ij}^2}{df_{error}}}, \qquad \text{[S3]}$$

where df_{error} is the degree of freedom given by

$$df_{error} = \sum_{i=1}^{2}\sum_{j=1}^{3} (n_{ij} - 1). \qquad \text{[S4]}$$

The 95% confidence levels (c.l.) for the calculated $\log(\tau/K_A)$ values are given by

$$\text{c.l.} = \log(\tau/K_A) \pm T(df_{error}, 0.975) \times (\text{SE}) \qquad \text{[S5]}$$

where SE is given by

$$\mathrm{SE} = S_{pooled}\sqrt{\frac{1}{n_{ij}}} \qquad \textbf{[S6]}$$

and T corresponds to a two-tailed t test with 95% confidence. For calculating the confidence levels for $\Delta\Delta\log(\tau/K_A)$, the same methodology (Eq. **S5**) is followed, except the SE is given by

$$\mathrm{SE} = \mathrm{S}_{pooled}\sqrt{\frac{1}{n_{WT}}+\frac{1}{n_{MUT}}+\frac{1}{n_{WT,ref}}+\frac{1}{n_{MUT,ref}}}, \qquad \textbf{[S7]}$$

where n refers to the number of experiments for the given pathway, and n_{ref} is the number of experiments for the reference pathway.

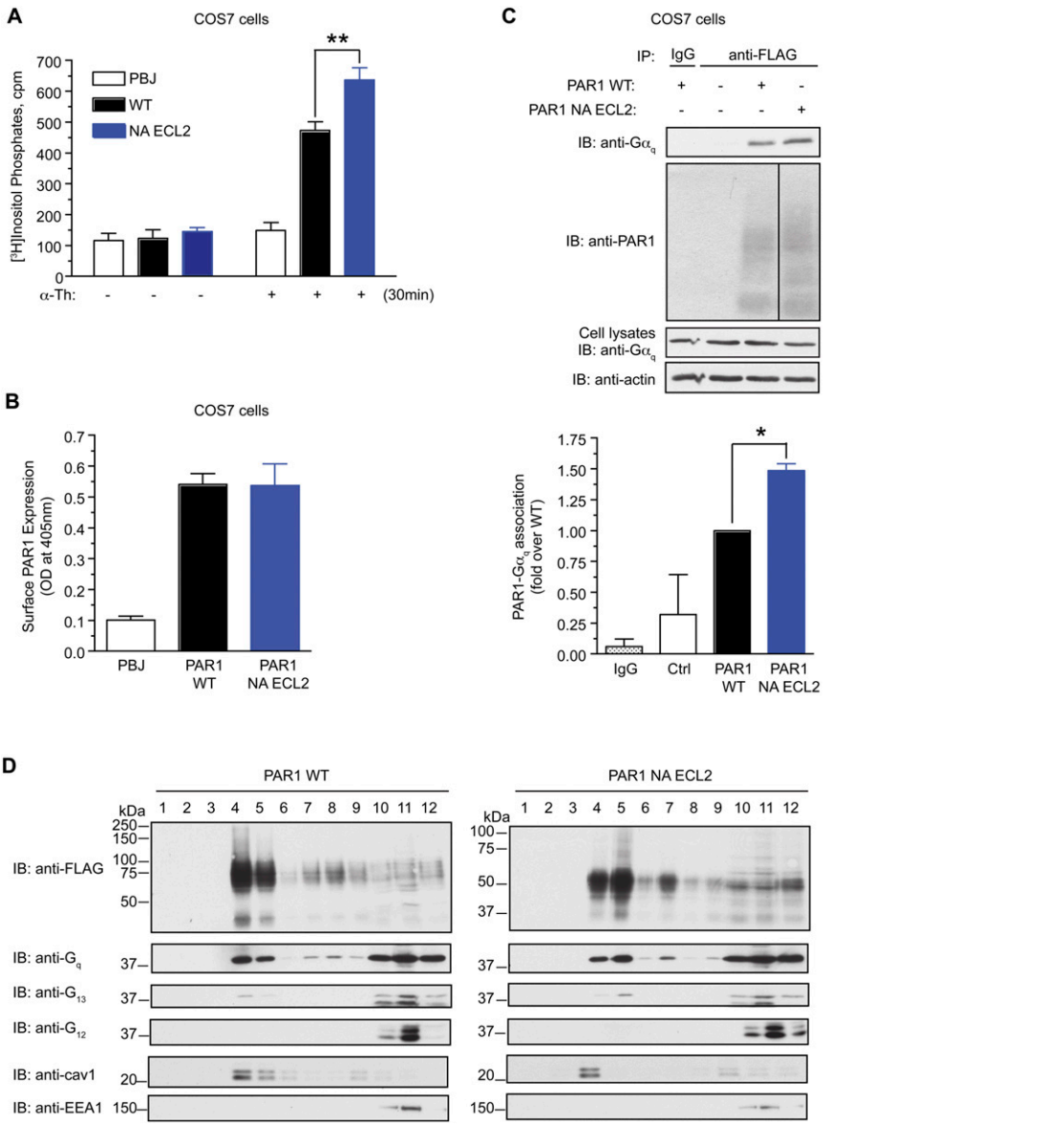

Fig. S1. PAR1 deficient in N-linked glycosylation at ECL2 exhibits enhanced $G\alpha_q$ association and PI hydrolysis in COS-7 cells but similar distribution in sucrose gradient fractionation. (*A*) COS-7 cells transiently transfected with PBJ vector, FLAG–PAR1 WT, or NA ECL2 mutant were labeled with *myo*-[^{3}H]inositol and treated with or without 10 nM α-Th for 30 min. The data shown (mean ± SD; $n = 3$) are representative of three independent experiments performed in triplicate and were significant (**$P < 0.01$). (*B*) PAR1 cell surface expression (mean ± SD; $n = 3$) was determined by ELISA. (*C*) COS-7 cells transiently coexpressing FLAG–PAR1 WT or NA ECL2 mutant with HA-tagged $G\alpha_q$ were lysed, immunoprecipitated, and immunoblotted as indicated. The data shown (mean ± SD; $n = 3$) are from three independent experiments and were significant (*$P < 0.05$). (*D*) FLAG–PAR1 WT or NA ECL2 mutant HeLa cells were lysed, and caveolin-1-enriched fractions were isolated by detergent-free sucrose gradient centrifugation. Aliquots representing each of the 12 fractions were immunoblotted as indicated.

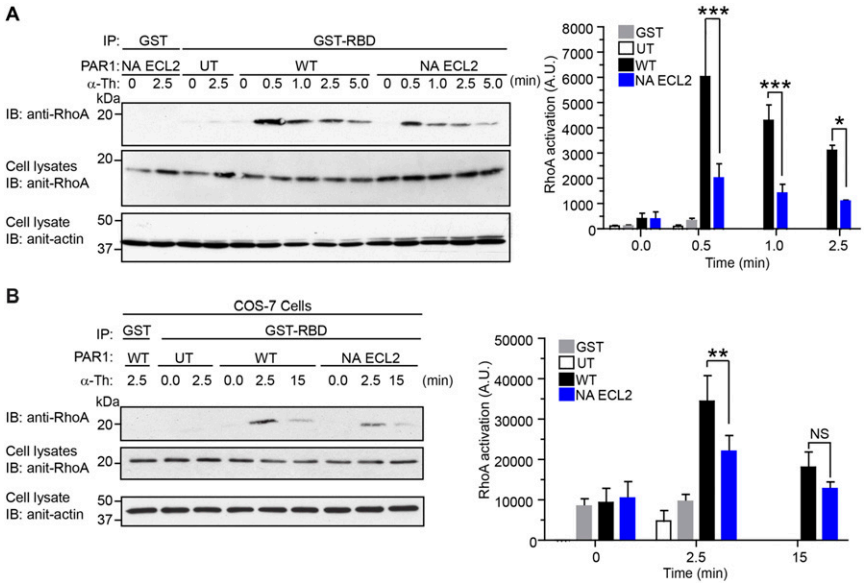

Fig. S2. Thrombin-induced RhoA activation in PAR1 WT and NA ECL2 mutant expressing HeLa and COS-7 cells. (*A*) FLAG–PAR1 WT or NA ECL2 mutant HeLa cells expressing similar amounts of cell surface expression (WT = 0.881 ± 0.016 and NA ECL2 = 0.818 ± 0.019, OD units) were treated with 10 nM α-Th, lysed and processed for GST-RBD pull-down assays, and activated RhoA was detected by immunoblotting. The data shown (mean ± SD; $n = 3$) were normalized to total RhoA and were significant (*$P < 0.05$; ***$P < 0.001$). (*B*) COS-7 cells transiently expressing similar cell surface levels of FLAG–PAR1 WT and NA ECL2 mutant (WT = 0.210 ± 0.016 and NA ECL2 = 0.196 ± 0.020, OD units) were treated with 10 nM α-Th, and RhoA activation was measured as described in *A*. Data (mean ± SD; $n = 3$) were normalized to total RhoA and were significant at 2.5 min (**$P < 0.01$). NS, not significant.

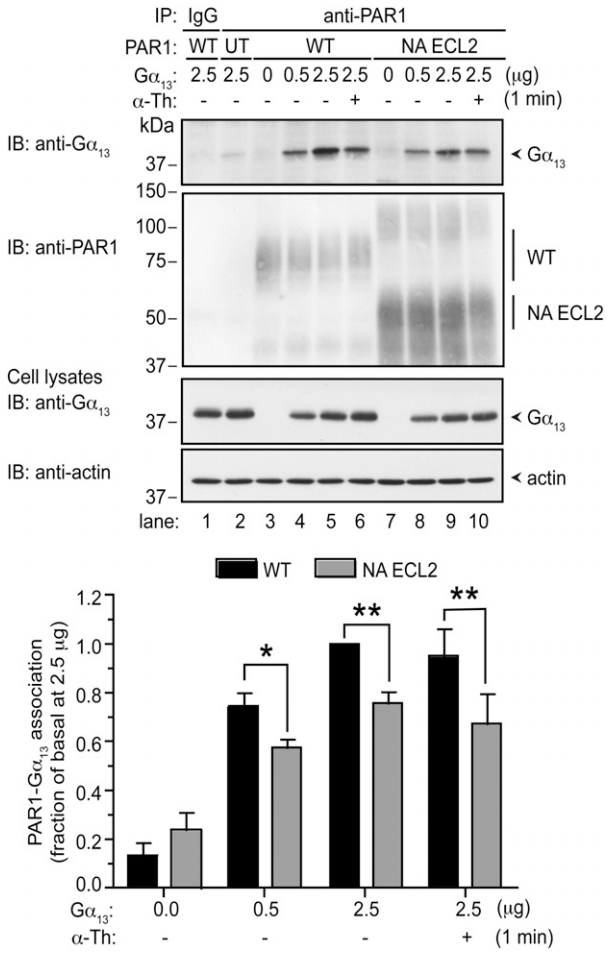

Fig. S3. PAR1 WT and NA ECL2 mutant differentially associate with $G\alpha_{13}$. FLAG–PAR1 WT or NA ECL2 mutant HeLa cells transiently transfected with $G\alpha_{13}$–EE were treated with or without 10 nM α-Th, lysed, PAR1 immunoprecipitated, and immunoblotted as indicated. The data shown (mean ± SD; $n = 3$) are representative of three independent experiments and were significant (*$P < 0.05$; **$P < 0.01$).

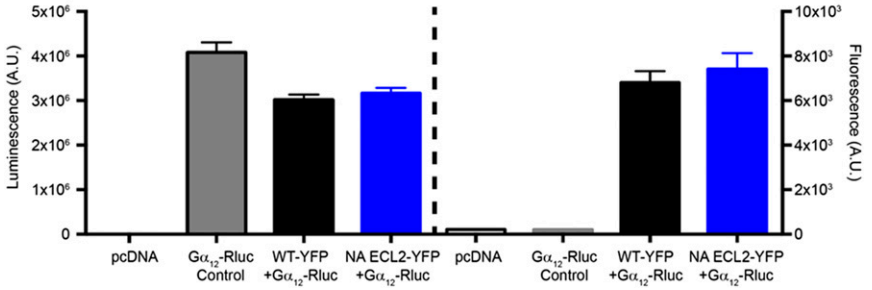

Fig. S4. PAR1 WT–YFP and NA ECL2–YFP and $G\alpha_{12}$–Rluc luminescence and fluorescence values. Total luminescence (*Left*) and fluorescence (*Right*) expressed as arbitrary units (A.U.) detected in PAR1 WT–YFP or NA ECL2–YFP coexpressed with $G\alpha_{12}$–Rluc or pcDNA vector transfected COS-7 cells. The data shown (mean ± SD; $n = 3$) are representative of three independent experiments.

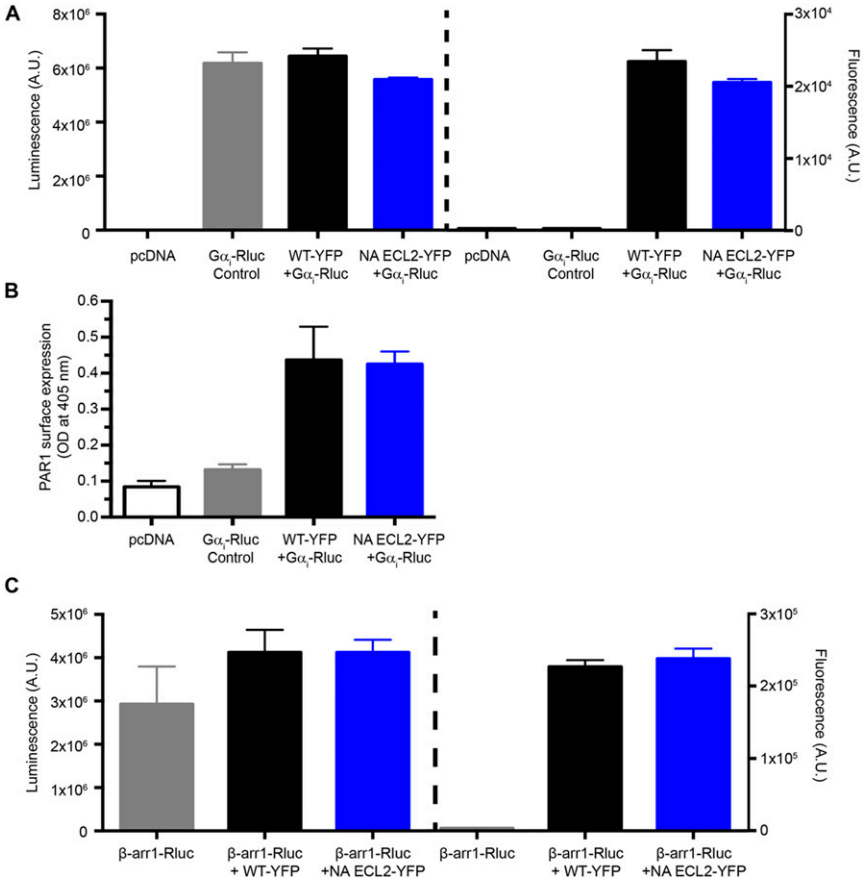

Fig. S5. PAR1 WT–YFP and NA ECL2 PAR1–YFP and $G\alpha_i$–Rluc or β-arrestin-1–Rluc expression, luminescence, and fluorescence. (*A*) Total luminescence (*Left*) and fluorescence (*Right*) expressed as A.U. from COS-7 cells coexpressing PAR1 WT–YFP or NA ECL2–YFP together with $G\alpha_i$–Rluc or pcDNA control. Data (mean ± SD; $n = 3$) are representative of three independent experiments. (*B*) PAR1 WT–YFP and NA ECL2–YFP cell surface expression in COS-7 cells coexpressing $G\alpha_i$–Rluc or pcDNA vector was determined by ELISA. (*C*) Total luminescence (*Left*) and fluorescence (*Right*) from COS-7 cells coexpressing PAR1 WT–YFP or NA ECL2–YFP and β-arrestin-1–Rluc. Data (mean ± SD; $n = 3$) are representative of three independent experiments.

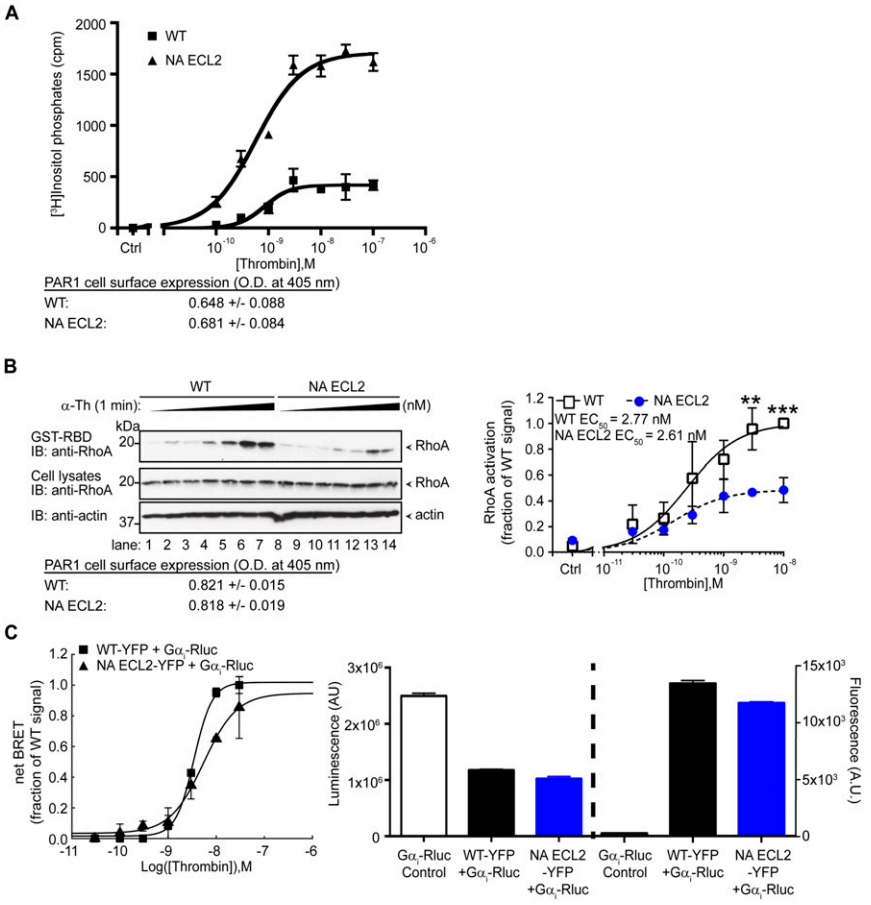

Fig. S6. PAR1 WT and NA ECL2 concentration–response curves. (*A*) PAR1 WT and NA ECL2 HeLa cells with comparable cell surface expression were labeled with *myo*-[^{3}H]inositol and left untreated (Ctrl) or treated with various concentrations of α-Th for 60 min at 37 °C. The data (mean ± SD; $n = 3$) are representative of three independent experiments. PAR1 surface expression (mean ± SD; $n = 3$) was determined by cell surface ELISA. (*B*) PAR1 WT and NA ECL2 expressed at similar levels in HeLa cells were treated without (Ctrl) or with various concentrations of α-Th for 1 min, and RhoA activation was determined. (*Left*) A representative RhoA GST-RBD pull-down immunoblot. (*Right*) The data (mean ± SD; $n = 4$) were normalized to total RhoA from four independent experiments. PAR1 surface expression (mean ± SD; $n = 3$) was determined by ELISA. (*C*) COS-7 cells transiently coexpressing PAR1 WT–YFP or NA ECL2–YFP and $G\alpha_i$–Rluc were left untreated (Ctrl) or treated with various concentrations of α-Th for 2.5 min and net BRET signal was determined. (*Left*) The data (mean ± SD; $n = 3$) are the net BRET signal from three independent experiments. (*Right*) Total luminescence and fluorescence PAR1 WT–YFP and NA ECL2–YFP coexpressed with $G\alpha_i$–Rluc.

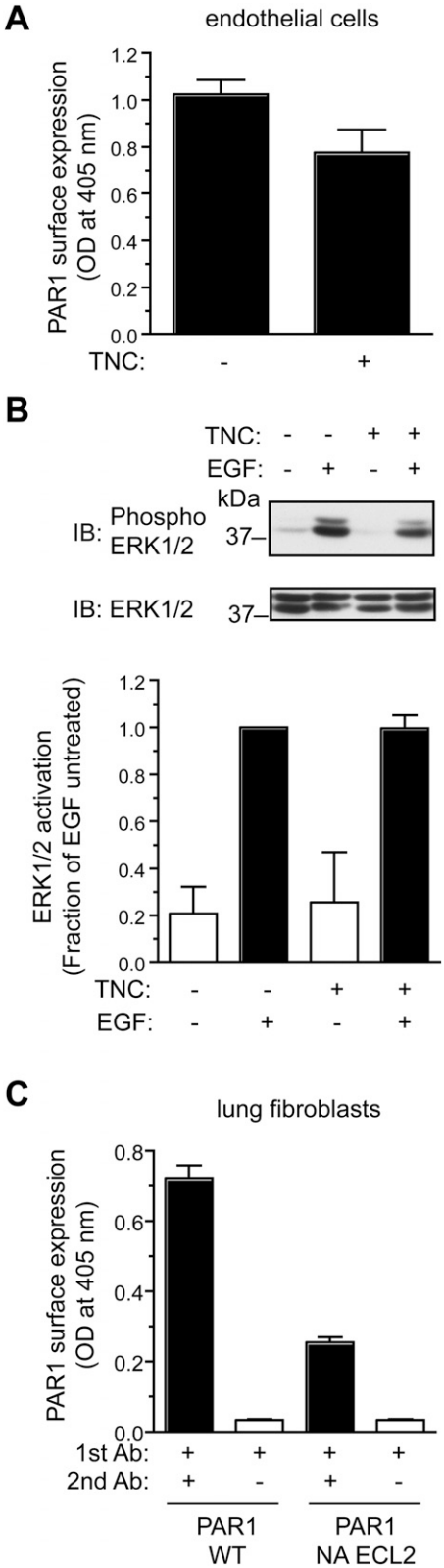

Fig. S7. Surface expression of PAR1 in endothelial cells and fibroblasts and EGF signaling. Endothelial cells expressing endogenous PAR1 were treated with or without 0.25 μg/mL TNC for 18 h at 37 °C. (*A*) PAR1 surface expression (mean ± SD; $n = 3$) was measured by ELISA. (*B*) Control and TNC-treated endothelial cells were serum starved for 1 h at 37 °C, then treated with or without 100 ng/mL EGF for 5 min at 37 °C. Cells were lysed, and lysates were immunoblotted with anti-phospho-ERK1/2 and anti-total-ERK1/2 antibodies. The data (mean ± SD; $n = 3$) are representative of three independent experiments. (*C*) FLAG–PAR1 WT and NA ECL2 mutant cell surface expression (mean ± SD; $n = 3$) in mouse lung *Par1*$^{-/-}$ fibroblasts was determined by ELISA using anti-PAR1 antibody (first Ab) and GAM-HRP (second Ab).

Table S1. Fitted parameters for each experimental concentration–response data for PAR1 WT and NA ECL2 mutant

Pathway	Receptor	Experiment	n	K_A	$\log(\tau/K_A)$	Mean $\log(\tau/K_A)$
RhoA	PAR1 WT	1	1.20	1.00E+00	9.07	9.54
		2	0.90	5.33E-09	9.66	
		3	1.20	1.94E-09	9.90	
	PAR1 NA ECL2	1	1.20	1.50E-09	8.60	9.09
		2	1.20	2.53E-10	9.50	
		3	0.90	3.23E-10	9.17	
PI hydrolysis	PAR1 WT	1	0.90	1.20E-09	8.44	8.53
		2	1.20	8.32E-10	8.67	
		3	1.20	7.47E-10	8.49	
	PAR1 NA ECL2	1	1.20	1.53E-08	8.96	9.04
		2	0.97	1.79E-08	9.21	
		3	1.20	1.53E-08	8.96	
G_i	PAR1 WT	1	1.20	9.60E-01	8.54	8.35
		2	1.20	1.00E+00	8.43	
		3	1.20	3.16E-08	8.13	
		4	1.20	1.08E-08	8.32	
	PAR1 NA ECL2	1	1.20	6.83E-09	8.24	8.14
		2	1.08	1.43E-07	8.23	
		3	1.20	9.03E-09	8.04	
		4	0.90	3.37E-07	8.05	

Table S2. Calculation of error estimates for $\log(\tau/K_A)$ values for the different pathways

Receptor	Pathway	Mean $\log(\tau/K_A)$	S_{ij}^2	n_{ij}	df_{error}	S_{pooled}	SE	T value	95% c.i.
PAR1 WT	RhoA	9.54	0.18	3			0.11		0.23
	PI Hydrolysis	8.53	0.01	3			0.11		0.23
	G_i	8.35	0.03	4	14.00	0.18	0.09	2.14	0.20
PAR1 NA ECL2	RhoA	9.09	0.21	3			0.11		0.23
	PI Hydrolysis	9.04	0.02	3			0.11		0.23
	G_i	8.14	0.01	4			0.09		0.20